



Journal of Applied and Computational Mechanics



Research Paper

Thermoelastic Modeling with Dual Porosity Interacting with an Inviscid Liquid

Rajesh Kumar¹, Vijayata Pathania², Vipin Gupta³, M.S. Barak⁴, Hijaz Ahmad^{5,6,7}

¹Department of Mathematics, Indira Gandhi University, Meerpur, 123401, India, Email: rajesh.math.rs@igu.ac.in

²Department of Mathematics, HPU Regional Centre, Dharamshala, 176218, India, Email: vpmsmrc@gmail.com

³Department of Mathematics, Indira Gandhi University, Meerpur, 123401, India, Email: vipin.math.rs@igu.ac.in

⁴Department of Mathematics, Indira Gandhi University, Meerpur, 123401, India, Email: ms_barak@igu.ac.in

⁵Department of Mathematics, Faculty of Science, Islamic University of Madinah, Medina, 42210, Saudi Arabia, Email: hahmad@iu.edu.sa

⁶Near East University, Operational Research Center in Healthcare, TRNC Mersin 10, Nicosia, 99138, Turkey, Email: hijaz.ahmad@neu.edu.tr

⁷Department of Computer Science and Mathematics, Lebanese American University, Beirut, Lebanon, Email: hijaz555@gmail.com

Received August 13 2023; Revised September 26 2023; Accepted for publication September 27 2023.

Corresponding author: H. Ahmad (ahmad.hijaz@uninettuno.it)

© 2023 Published by Shahid Chamran University of Ahvaz

Abstract. This study introduces a two-dimensional thermoelastic model for a homogeneous isotropic half-space with double porosity underlying an inviscid liquid half-space featuring temperature variations. The model incorporates the three-phase lag (TPL) heat equation and reveals that in the solid half-space, four coupled longitudinal waves intertwine with one uncoupled transverse wave, while one mechanical wave ripples through the liquid half-space. The investigation highlights dispersion, attenuation, and other effects affected by the thermal properties and the presence of voids. Using plane wave solutions and boundary conditions at the interface, a concise expression for the frequency equation of the model has been derived. Furthermore, the magnitudes of the displacements in the solid half-space and liquid half-spaces, the temperature change, and the volume fractional fields at the interface have been precisely determined. In the graphical section, computer-simulated results of various wave profiles for magnesium crystal material have been generated for different heat conduction thermoelastic models. The study's implications span various fields, such as hydrology, engineering, ultrasonics, navigation, and electronics.

Keywords: Isotropic, double porosity, thermoelasticity, three-phase lag, inviscid liquid, varying temperature.

1. Introduction

It is widely acknowledged that the classical theory of heat conduction, which depends on Fourier's law, entails a prediction of an infinite rate of heat propagation. To solve the predicament of this unbounded thermal transmission velocity within the classical coupled thermoelasticity framework, Lord and Shulman [1] introduced the pioneering generalized theory featuring a single relaxation time. Through the incorporation of this relaxation time, the heat conduction law given by Fourier supplants the Maxwell-Cattaneo law in the Lord-Shulman theory. Green and Lindsay [2] significantly enhanced the thermal conduction principle described by Fourier's law by identifying a hyperbolic equation with two thermal relaxation durations. Without energy dissipation, a thermoelasticity theory was developed by Green and Naghdi [3], which substitutes the Fourier law with a correlation between heat flow rate and temperature gradient. Tzou [4] introduced the dual-phase-lag (DPL) generalized thermoelastic theory. The heat flux vector and temperature gradient were established by Tzou as two separate time delays. Temporal delay accentuates the expeditious transitory characteristics of microstructural interchanges stemming from the transient attributes of thermal inertia. Roy Choudhari [5] introduced the latest thermoelasticity theory, known as three phase-lag (TPL) thermoelasticity theory using the thermal displacement gradient concomitant with the inclusion of time delay.

Porous materials have many uses in the fields together with bone mechanics, material science, geophysics, medicine, the manufacturing of medical devices, electrical communications, chemical engineering, the petroleum industry, environmental protection, etc. While the material's pores are what generate the macroporosity, the fissures in the material are what cause the microporosity in the double porous structure. Many various types of biological, geological, and synthetic materials have thermoelastic materials with voids, which are helpful in both functional and structural forms. Nunziato and Cowin [6] used nonlinear theory to investigate the existence of voids or cavities within an elastic material. Using the multi-porous material, Aifantis [7] researched a new degree of freedom for each of the material's particles using the multi-porous material, which was specified as a percentage of the elementary volume. Iesan [8] created the linear theory of thermoelastic porous materials, which incorporates thermal properties and produced theorems on the uniqueness of solutions, reciprocity, and variational characterization. Svanadze [9] Obtained fundamental solution system equations governing steady oscillation's elementary functions and further established fundamental properties.

The CT and LS theory was used by Sharma et al. [10] to provide a description of surface waves propagating in a thermoelastic solid medium that is in contact with an inviscid liquid medium at distinct temperatures. A theory of double-porous solids was introduced



by Iesan and Quintanilla [11], who concluded that in equilibrium, this theory differs from the conventional theory of double-porous elastic materials. To find the only solution to the boundary value issue in a double porous elastic model, Straughan [12] constructed a novel functional. Kumar et al. [13] conducted an inquiry into the phenomena of refraction and reflection pertaining to planar harmonic waves in an elastic half-space in contact with a material characterized by dual permeability and double porosity. Kumar and Vohra [14] investigated the variables influencing the stress and temperature distribution brought on by moving thermal and mechanical sources in a dual porous thermoelastic solid. Using the generalized theories of thermoelasticity, Sharma and Pathania [15] made an effort to analyze the waves in an elasto-thermal plate in contact with a half-space or layer of non-viscous fluid on each face of the plate. Singh et al. [16] studied transmission of the plane wave in a double porous thermoelastic solid and concluded that the linked longitudinal wave is due to the particle displacement, thermal signal, and volume fractions of voids. The transmission of thermoelastic waves with a certain wavelength and twofold porosity was studied by Chirita and Arusoae [17]. Pathania and Dhiman [18] investigated wave propagation in a poro-thermoelastic thin plate. Svanadze [19] investigated a linear coupled model of a double porous elastic material that takes into account both the volume proportion of voids and Darcy's law. A thermoelastic homogenous, anisotropic, semi-infinite material linked with an inviscid fluid was hypothesized to be affected by the void by Pathania and Joshi [20]. Gupta and his coworker [21–24] investigated various wave propagation problems in elastic, inviscid fluid, thermoelastic and piezoelectric materials.

Biswas [25] studied the propagation of plane waves in an isotropic porous thermoelastic media using the DPL model. In a two-dimensional porous media, Hobiny and Abbas [26] suggested a model for thermoelastic waves and calculated the various wave profiles. In their discussion of the TPL model's stability, Quintanilla and Racke [27] took into account the two distinct applications of the law of heat conduction. Shaw and Mukhopadhyay [28] went into more detail on how Rayleigh waves move through a micropolar isotropic thermoelastic material using TPL theory. Kalkal et al. [29] investigated the gravitational effects on the thermomechanical interactions in an isotropic double porous half-space using the TPL model. In the framework of a TPL model, Biswas [30] presented a precise analysis of the free vibrations of an isotropic, homogeneous cylindrical panel containing pores.

While previous literature has explored the impact of double porosity on thermoelastic wave propagation in semi-infinite materials, the influence of an inviscid liquid with variable temperature on such materials remains unexplored. This paper investigates the interaction of plane waves at the interface of a homogeneous isotropic double porous thermoelastic solid and a non-viscous liquid at varying temperatures using the TPL model. Through normal mode analysis and the application of interfacial mechanical and thermal conditions, the frequency equation is derived. Numerical results are presented to illustrate and demonstrate various plane wave profiles with different phase lags. The findings of this study have broad implications for engineering fields, including soil dynamics, seismology, earthquake engineering, geophysics, and more.

2. Formulation of the Problem

Now, consider a double porous thermoelastic solid half-space that is isotropic and homogeneous at constant temperature θ_0 with an inviscid liquid half-space with varying temperature. The coordinate system (x, y, z) has its origin O at the interface of two mediums, i.e., at $z = 0$. As described in Figure 1, the z^+ direction is vertically downward in the double porous thermoelastic half-space. It is assumed that the solutions are independent of the y -axis and depend on x, z , and time t . The displacement along the positive propagation direction x is assumed to be harmonic. The disturbance is restricted near the region $z = 0$ and dies out as $z \rightarrow \pm\infty$.

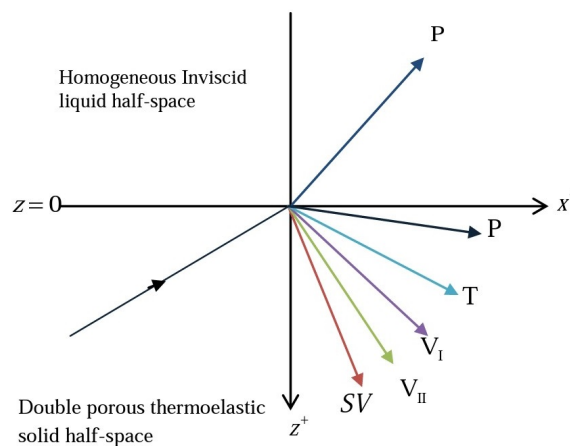


Fig. 1. Geometry of the problem

Following Iesan and Quintanilla [11], Sharma et al. [10], and Roy Choudhuri [5], the field equations for the solid medium with the TPL model in contact with inviscid liquid at a varying temperature have been given as

$$(\lambda + 2\mu) \frac{\partial^2 u}{\partial x^2} + \lambda \frac{\partial^2 w}{\partial x \partial z} + \mu \left(\frac{\partial^2 u}{\partial z^2} + \frac{\partial^2 w}{\partial x \partial z} \right) + b \frac{\partial \phi}{\partial x} + d \frac{\partial \psi}{\partial x} - \beta \frac{\partial \theta}{\partial x} = \rho \frac{\partial^2 u}{\partial t^2} \tag{1}$$

$$(\lambda + \mu) \frac{\partial u}{\partial x \partial z} + \mu \frac{\partial^2 w}{\partial x^2} + (\lambda + 2\mu) \frac{\partial^2 w}{\partial z^2} + b \frac{\partial \phi}{\partial z} + d \frac{\partial \psi}{\partial z} - \beta \frac{\partial \theta}{\partial z} = \rho \frac{\partial^2 w}{\partial t^2} \tag{2}$$

$$-b \left(\frac{\partial u}{\partial x} + \frac{\partial w}{\partial z} \right) + \alpha \left(\frac{\partial^2 \phi}{\partial x^2} + \frac{\partial^2 \phi}{\partial z^2} \right) - \alpha_1 \phi + b_1 \left(\frac{\partial^2 \psi}{\partial x^2} + \frac{\partial^2 \psi}{\partial z^2} \right) - \alpha_3 \psi + \gamma_1 \theta = \chi_1 \frac{\partial^2 \phi}{\partial t^2} \tag{3}$$

$$-d \left(\frac{\partial u}{\partial x} + \frac{\partial w}{\partial z} \right) + b_1 \left(\frac{\partial^2 \phi}{\partial x^2} + \frac{\partial^2 \phi}{\partial z^2} \right) - \alpha_3 \phi + \gamma \left(\frac{\partial^2 \psi}{\partial x^2} + \frac{\partial^2 \psi}{\partial z^2} \right) - \alpha_2 \psi + \gamma_2 \theta = \chi_2 \frac{\partial^2 \psi}{\partial t^2} \tag{4}$$

$$K^* \left(1 + \tau_v \frac{\partial}{\partial t} \right) \left(\frac{\partial^2 T}{\partial x^2} + \frac{\partial^2 T}{\partial z^2} \right) + K \left(1 + \tau_T \frac{\partial}{\partial t} \right) \left(\frac{\partial^3 \theta}{\partial x^2 \partial t} + \frac{\partial^3 \theta}{\partial z^2 \partial t} \right)$$



$$= \left(1 + \tau_q \frac{\partial}{\partial t} + \frac{\tau_q^2}{2} \frac{\partial^2}{\partial t^2} \right) \left[\beta \theta_0 \left(\frac{\partial^3 u}{\partial x \partial t^2} + \frac{\partial^3 w}{\partial z \partial t^2} \right) + \gamma_1 \theta_0 \frac{\partial^2 \phi}{\partial t^2} + \gamma_2 \theta_0 \frac{\partial^2 \psi}{\partial t^2} + \rho C_e \frac{\partial^2 \theta}{\partial t^2} \right] \quad (5)$$

$$\lambda_L \left(\frac{\partial^2 u_L}{\partial x^2} + \frac{\partial^2 w_L}{\partial z \partial x} \right) - \beta_L^* \frac{\partial \theta_L}{\partial x} = \rho_L \frac{\partial^2 u_L}{\partial t^2} \quad (6)$$

$$\lambda_L \left(\frac{\partial^2 u_L}{\partial x \partial z} + \frac{\partial^2 w_L}{\partial z^2} \right) - \beta_L^* \frac{\partial \theta_L}{\partial z} = \rho_L \frac{\partial^2 w_L}{\partial t^2} \quad (7)$$

$$\beta_L^* \theta_0^* \left(\frac{\partial u_L}{\partial x} + \frac{\partial w_L}{\partial z} \right) = -\rho_L C_e^* \theta_L \quad (8)$$

Subscript L stands for parameters of liquid half-space. The subscripts denoted by a superposed dot “.” and a comma “,” represent time and partial derivative, respectively.

For convenience, let us take into account the subsequent dimensionless parameters.

$$(x', z') = \frac{\omega^*}{c_1} (x, z), \quad (u', w') = \frac{\rho \omega^* c_1}{\beta T_0} (u, w), \quad (t', \tau'_q, \tau'_T, \tau'_\nu) = \omega^* (t, \tau_q, \tau_T, \tau_\nu), \quad (T', T'_L) = \frac{1}{T_0} (T, T_L) \\ (\varphi', \psi') = \frac{\omega^{*2} \chi_1}{c_1^2} (\varphi, \psi), \quad (u'_L, w'_L) = \frac{\rho \omega^* c_1}{\beta T_0} (u_L, w_L) \quad (9)$$

Substituting the quantities defined in Eq. (2.) in the Eq. (1)-(8), the basic equations have been reduced in dimension-less form as (the primes are dropped for convenience)

$$\frac{\partial^2 u}{\partial x^2} + \eta^2 \frac{\partial^2 u}{\partial z^2} + (1 - \eta^2) \frac{\partial^2 w}{\partial x \partial z} + l_1 \frac{\partial \phi}{\partial x} + l_2 \frac{\partial \psi}{\partial x} - \frac{\partial \theta}{\partial x} = \frac{\partial^2 u}{\partial t^2} \quad (10)$$

$$(1 - \eta^2) \frac{\partial^2 u}{\partial x \partial z} + \eta^2 \frac{\partial^2 w}{\partial x^2} + \frac{\partial^2 w}{\partial z^2} + l_1 \frac{\partial \phi}{\partial z} + l_2 \frac{\partial \psi}{\partial z} - \frac{\partial \theta}{\partial z} = \frac{\partial^2 w}{\partial t^2} \quad (11)$$

$$-l_4 \left(\frac{\partial u}{\partial x} + \frac{\partial w}{\partial z} \right) + \frac{\partial^2 \varphi}{\partial x^2} + \frac{\partial^2 \varphi}{\partial z^2} - l_5 \phi + l_3 \left(\frac{\partial^2 \psi}{\partial x^2} + \frac{\partial^2 \psi}{\partial z^2} \right) - l_6 \psi + l_7 \theta = \frac{1}{\eta_1^2} \frac{\partial^2 \varphi}{\partial t^2} \quad (12)$$

$$-l_9 \left(\frac{\partial u}{\partial x} + \frac{\partial w}{\partial z} \right) + \frac{\partial^2 \varphi}{\partial x^2} + \frac{\partial^2 \varphi}{\partial z^2} - l_{10} \varphi + l_8 \left(\frac{\partial^2 \psi}{\partial x^2} + \frac{\partial^2 \psi}{\partial z^2} \right) - l_{11} \psi + l_{12} \theta = \frac{1}{\eta_2^2} \frac{\partial^2 \psi}{\partial t^2} \quad (13)$$

$$l_{15} \left(1 + \tau_\nu \frac{\partial}{\partial t} \right) \left(\frac{\partial^2 \theta}{\partial x^2} + \frac{\partial^2 \theta}{\partial z^2} \right) + \left(1 + \tau_T \frac{\partial}{\partial t} \right) \left(\frac{\partial^3 \theta}{\partial x^2 \partial t} + \frac{\partial^3 \theta}{\partial z^2 \partial t} \right) \\ = \left(1 + \tau_q \frac{\partial}{\partial t} + \frac{\tau_q^2}{2} \frac{\partial^2}{\partial t^2} \right) \left(\varsigma_T \left(\frac{\partial^3 u}{\partial t^2 \partial x} + \frac{\partial^3 w}{\partial t^2 \partial z} \right) + l_{13} \frac{\partial^2 \varphi}{\partial t^2} + l_{14} \frac{\partial^2 \psi}{\partial t^2} + \frac{\partial^2 \theta}{\partial t^2} \right) \quad (14)$$

$$\frac{\partial^2 u_L}{\partial x^2} + \frac{\partial^2 w_L}{\partial x \partial z} - \frac{\bar{\beta}_L \rho c_1^2}{\lambda_L} \frac{\partial \theta_L}{\partial x} = \frac{1}{\eta_L^2} \frac{\partial^2 u_L}{\partial t^2} \quad (15)$$

$$\frac{\partial^2 u_L}{\partial x \partial z} + \frac{\partial^2 w_L}{\partial z^2} - \frac{\bar{\beta}_L \rho c_1^2}{\lambda_L} \frac{\partial \theta_L}{\partial z} = \frac{1}{\eta_L^2} \frac{\partial^2 w_L}{\partial t^2} \quad (16)$$

$$\rho_L \varsigma_L \left(\frac{\partial u_L}{\partial x} + \frac{\partial w_L}{\partial z} \right) = -\frac{\rho \bar{\beta}_L}{\eta_L^2} \theta_L \quad (17)$$

where

$$\eta^2 = \frac{c_2^2}{c_1^2}, \quad \eta_1^2 = \frac{c_3^2}{c_1^2}, \quad \eta_2^2 = \frac{c_4^2}{c_1^2}, \quad \eta_L^2 = \frac{c_L^2}{c_1^2}, \quad \beta = (3\lambda + 2\mu) \alpha_t, \quad \beta_L^* = 3\lambda_L \alpha_t^*, \quad \varsigma_T = \frac{\beta^2 \theta_0}{\rho K \omega^*}, \quad \varsigma_L = \frac{\beta_L^* \theta_0^*}{C_e^* \rho_L^2 c_L^2}, \quad c_1^2 = \frac{\lambda + 2\mu}{\rho}, \quad c_2^2 = \frac{\mu}{\rho}, \\ c_3^2 = \frac{\alpha}{\chi_1}, \quad c_4^2 = \frac{b_1}{\chi_2}, \quad \omega^* = \frac{C_e \rho c_1^2}{K}, \quad \bar{\beta}_L = \frac{\beta_L^*}{\beta}, \quad l_1 = \frac{b c_1^2}{\omega^{*2} \chi_1 \beta \theta_0}, \quad l_2 = \frac{d c_1^2}{\omega^{*2} \chi_1 \beta \theta_0}, \quad l_3 = \frac{b_1}{\alpha}, \quad l_4 = \frac{\beta \theta_0 \chi_1 b}{\rho c_1^2 \alpha}, \quad l_5 = \frac{\alpha_1 c_1^2}{\alpha \omega^{*2}}, \quad l_6 = \frac{\alpha_3 c_1^2}{\alpha \omega^{*2}}, \\ l_7 = \frac{\gamma_1 \theta_0 \chi_1}{\alpha}, \quad l_8 = \frac{\gamma}{b_1}, \quad l_9 = \frac{\beta \theta_0 \chi_1 d}{\rho c_1^2 b_1}, \quad l_{10} = \frac{\alpha_3 c_1^2}{\omega^{*2} b_1}, \quad l_{11} = \frac{\alpha_2 c_1^2}{\omega^{*2} b_1}, \quad l_{12} = \frac{\gamma_2 \theta_0 \chi_1}{b_1}, \quad l_{13} = \frac{\gamma_1 c_1^4}{\omega^{*3} K \chi_1}, \quad l_{14} = \frac{\gamma_2 c_1^4}{\omega^{*3} K \chi_1}, \quad l_{15} = \frac{K^*}{K \omega^*}.$$

Here, ω^* denotes the distinctive frequency of the thermoelastic double porous medium, c_1 , c_2 , c_3 and c_4 represent the longitudinal waves, transverse waves, and volume fraction field velocities of type-I, II voids, respectively.

With the utilization of the Helmholtz decomposition theorem, the displacement components are defined by

$$u = \frac{\partial F}{\partial x} + \frac{\partial N}{\partial z}, \quad w = \frac{\partial F}{\partial z} - \frac{\partial N}{\partial x} \quad (18)$$

where N and F respectively denote the vector and scalar function for the shear and longitudinal waves.

Since there is no shear motion in the inviscid liquid, the shear mode of the inviscid liquid vanishes. Thus the displacement components in the liquid half-space may be defined as

$$u_L = \frac{\partial F_L}{\partial x}, \quad w_L = \frac{\partial F_L}{\partial z} \quad (19)$$

where F_L represents the scalar function for inviscid liquid.

Substituting the Eqs. (18)-(19) in the Eqs. (10)-(17), we get

$$\frac{\partial^2 F}{\partial x^2} + \frac{\partial^2 F}{\partial z^2} + l_1 \varphi + l_2 \psi - \theta = \frac{\partial^2 F}{\partial t^2} \quad (20)$$



$$\left(\frac{\partial^2 N}{\partial x^2} + \frac{\partial^2 N}{\partial z^2}\right) = \frac{1}{\eta^2} \frac{\partial^2 N}{\partial t^2} \tag{21}$$

$$-l_4 \left(\frac{\partial^2 F}{\partial x^2} + \frac{\partial^2 F}{\partial z^2}\right) + \frac{\partial^2 \varphi}{\partial x^2} + \frac{\partial^2 \varphi}{\partial z^2} - l_5 \varphi + l_3 \left(\frac{\partial^2 \psi}{\partial x^2} + \frac{\partial^2 \psi}{\partial z^2}\right) - l_6 \psi + l_7 \theta = \frac{1}{\eta_1^2} \frac{\partial^2 \varphi}{\partial t^2} \tag{22}$$

$$-l_9 \left(\frac{\partial^2 F}{\partial x^2} + \frac{\partial^2 F}{\partial z^2}\right) + \frac{\partial^2 \varphi}{\partial x^2} + \frac{\partial^2 \varphi}{\partial z^2} - l_{10} \varphi + l_8 \left(\frac{\partial^2 \psi}{\partial x^2} + \frac{\partial^2 \psi}{\partial z^2}\right) - l_{11} \psi + l_{12} \theta = \frac{1}{\eta_2^2} \frac{\partial^2 \psi}{\partial t^2} \tag{23}$$

$$l_{15} \left(1 + \tau_\nu \frac{\partial}{\partial t}\right) \left(\frac{\partial^2 \theta}{\partial x^2} + \frac{\partial^2 \theta}{\partial z^2}\right) + \left(1 + \tau_T \frac{\partial}{\partial t}\right) \left(\frac{\partial^3 \theta}{\partial x^2 \partial t} + \frac{\partial^3 \theta}{\partial z^2 \partial t}\right) \\ = \left(1 + \tau_q \frac{\partial}{\partial t} + \frac{\tau_q^2}{2} \frac{\partial^2}{\partial t^2}\right) \left(\varsigma_T \left(\frac{\partial^3 F}{\partial t^2 \partial x} + \frac{\partial^3 F}{\partial t^2 \partial z}\right) + l_{13} \frac{\partial^2 \varphi}{\partial t^2} + l_{14} \frac{\partial^2 \psi}{\partial t^2} + \frac{\partial^2 \theta}{\partial t^2}\right) \tag{24}$$

$$\frac{\partial^2 F_L}{\partial x^2} + \frac{\partial^2 F_L}{\partial z^2} = \frac{1}{\eta_L^2 (1 + \varsigma_L)} \frac{\partial^2 F_L}{\partial t^2} \tag{25}$$

$$\theta_L = -\frac{\varsigma_L \rho_L}{\rho \beta_L (1 + \varsigma_L)} \frac{\partial^2 F_L}{\partial t^2} \tag{26}$$

Here, ς_T and ς_L denote the thermomechanical coupling in the solid and inviscid liquid half-spaces. The assumption has been made that the liquid is a hypothetical thermally non-conducting solid to get a temperature relation (26). Also, it is observed that the Eqs. (20), (22), (23), and (24) are coupled in the potential functions F, φ, ψ and θ . Hence, the thermal characteristics and parameters of both void types exert an influence on the interconnected wave system. Equation (21) is uncoupled in the potential function N and represents the shear wave equation. Equation (25) is uncoupled in the potential function F_L for the liquid medium.

3. Solution of the Problem

To tackle Eqs. (20)-(25), we proceed by assuming that the solution adopts the following form:

$$(F, N, \varphi, \psi, \theta, F_L) = \{\bar{F}(z), \bar{N}(z), \bar{\varphi}(z), \bar{\psi}(z), \bar{\theta}(z), \bar{F}_L(z)\} \exp\{ik(x - ct)\} \tag{27}$$

Here, $\omega(\omega' = \omega/\omega^*)$ is the angular frequency, $c = \omega/k (c' = c/c_1)$ is non-dimensional phase velocity, k is the wave number, $\bar{F}(z), \bar{N}(z), \bar{\varphi}(z), \bar{\psi}(z), \bar{\theta}(z), \bar{F}_L(z)$ are the function denoting the amplitude of waves.

Introducing the Eq. (27) in Eqs. (20)-(26) and suppressing the bars, we get

$$(n^2 + d_{11}) F + l_1 \varphi + l_2 \psi - \theta = 0 \tag{28}$$

$$(-l_4 n^2 + d_{31}) F + (n^2 + d_{32}) \varphi + (l_3 n^2 + d_{33}) \psi + l_7 \theta = 0 \tag{29}$$

$$(-l_9 n^2 + d_{41}) F + (n^2 + d_{42}) \varphi + (l_8 n^2 + d_{43}) \psi + l_{12} \theta = 0 \tag{30}$$

$$(d_{51} n^2 + d_{52}) F + d_{53} \varphi + d_{54} \psi + (d_{55} n^2 + d_{56}) \theta = 0 \tag{31}$$

$$(n^2 + d_{21}) N = 0 \tag{32}$$

$$(n^2 + d_{61}) F_L = 0 \tag{33}$$

$$\theta_L = S_L F_L \tag{34}$$

where

$$d_{11} = \omega^2 - k^2, \quad d_{21} = (\omega^2/\eta^2) - k^2, \quad d_{31} = l_4 k^2, \quad d_{32} = (\omega^2/\eta_1^2) - k^2 - l_5, \quad d_{33} = -l_3 k^2 - l_6, \quad d_{41} = l_9 k^2, \quad d_{42} = -k^2 - l_{10}, \\ d_{43} = (\omega^2/\eta_2^2) - l_8 k^2 - l_{11}, \quad d_{51} = t_q^* \varsigma_T \omega^2, \quad d_{52} = -k^2 d_{51}, \quad d_{53} = t_q^* \omega^2 l_{13}, \quad d_{54} = t_q^* \omega^2 l_{14}, \quad d_{55} = a_{15} t_\nu + t_T, \quad d_{56} = -k^2 d_{55} + \omega^2 t_q^*, \\ d_{61} = [\omega^2/\eta^2 (1 + \varsigma_L)] - k^2, \quad t_q = i\omega^{-1} + \tau_q, \quad t_T = i\omega^{-1} + \tau_T, \quad t_\nu = i\omega^{-1} + \tau_\nu, \quad t_q^* = t_q - i\omega(\tau_q^2/2), \quad S_L = \frac{\varsigma_L \rho_L \omega^2}{\rho \beta_L (1 + \varsigma_L)}.$$

In case the determinant of the coefficient matrix is zero, the set of homogeneous Eqs. (28)-(31) will possess a non-trivial solution, which leads to the roots of the characteristics equation as

$$n_j^2 = k^2 (1 - \lambda_j^2 c^2); \quad j = 1, 2, 3, 4, 5, 6 \tag{35}$$

where $\lambda_j^2; j = 1, 2, 3, 4$ are the roots of the characteristics equation

$$J_0 D^4 + J_1 D^3 + J_2 D^2 + J_3 D + J_4 = 0. \tag{36}$$

Here, the coefficients J_0, J_1, J_2, J_3, J_4 are given in the Appendix A. These coefficients have complex values. Consequently, the characteristic roots of the Eq. (36) are also complex in nature.

Also, from Eqs. (32) and (33), we have

$$\lambda_5^2 = \frac{1}{\eta^2} \tag{37}$$

$$\lambda_6^2 = \frac{1}{\eta^2 (1 + \varsigma_L)} \tag{38}$$

These $n_j^2; j = 1, 2, 3, 4$ correspond to the coupled system of four compressional waves produced due to variations in both types of void volume fraction fields, thermal changes, and mechanical stresses. Leftover roots $n_j^2; j = 5, 6$ are for the one decoupled shear wave in solid and one longitudinal wave in liquid half-space, respectively.



4. Amplitude Ratios

In this paper, only the surface waves have been studied; thus, the motion of waves is restricted to the interface $z = 0$ of the solid half-space and liquid half-spaces. Thus the prescribed solution for the double porous solid medium with thermal properties ($0 < z < \infty$) satisfying the radiation conditions $Re(n_q \geq 0, q = 1, 2, 3, 4, 5)$ can be attained as

$$(F, \varphi, \psi, \theta) = \sum_{q=1}^4 (1, A_q, B_q, C_q) E_q \exp \{ \iota k (x - ct) - n_q z \} \quad (39)$$

$$N = E_5 \exp \{ \iota k (x - ct) - n_5 z \} \quad (40)$$

The formal solution for the inviscid liquid half-space ($-\infty < z < 0$), satisfying the radiation condition $Re(n_6) \geq 0$ is given by

$$F_L = E_6 \exp \{ \iota k (x - ct) + n_6 z \} \quad (41)$$

$$\theta_L = S_L E_6 \exp \{ \iota k (x - ct) + n_6 z \} \quad (42)$$

where A_q, B_q, C_q represent the coupling constraints, which are specified in the Appendix B. Also E_1, E_2, E_3, E_4 , and E_5 represent the amplitudes of linked compressional and shear waves in the solid and E_6 represent the amplitude of compressional waves in an inviscid fluid, respectively.

5. Special Cases of the Heat Equation

- If $K^* = \tau_q = \tau_T = \tau_\nu = 0$, then the heat conduction Eq. (14) is reduced to the Biot theory of classical thermoelasticity [31]

$$\varsigma_T \left(\frac{\partial^2 u}{\partial x \partial t} + \frac{\partial^2 w}{\partial z \partial t} \right) + l_{13} \frac{\partial \varphi}{\partial t} + l_{14} \frac{\partial \psi}{\partial t} + \frac{\partial \theta}{\partial t} = \frac{\partial^2 \theta}{\partial x^2} + \frac{\partial^2 \theta}{\partial z^2} \quad (43)$$

- The Lord and Shulman (LS) model of thermoelasticity [1] is obtained from Eq. (14) if $\tau_q = \tau_0 > 0$ and $K^* = \tau_T = \tau_\nu = 0$ as

$$\left(1 + \tau_0 \frac{\partial}{\partial t} \right) \left(\varsigma_T \left(\frac{\partial^2 u}{\partial x \partial t} + \frac{\partial^2 w}{\partial z \partial t} \right) + l_{13} \frac{\partial \varphi}{\partial t} + l_{14} \frac{\partial \psi}{\partial t} + \frac{\partial \theta}{\partial t} \right) = \frac{\partial^2 \theta}{\partial x^2} + \frac{\partial^2 \theta}{\partial z^2} \quad (44)$$

- The generalized heat conduction equation of Tzou's DPL theory [4] is acquired from Eq. (14) when $\tau_\nu = K^* = 0$, and proposed as

$$\left(1 + \tau_0 \frac{\partial}{\partial t} + \frac{\tau_q^2}{2} \frac{\partial^2}{\partial t^2} \right) \left(\varsigma_T \left(\frac{\partial^2 u}{\partial x \partial t} + \frac{\partial^2 w}{\partial z \partial t} \right) + l_{13} \frac{\partial \varphi}{\partial t} + l_{14} \frac{\partial \psi}{\partial t} + \frac{\partial \theta}{\partial t} \right) = \left(1 + \tau_T \frac{\partial}{\partial t} \right) \left(\frac{\partial^2 \theta}{\partial x^2} + \frac{\partial^2 \theta}{\partial z^2} \right) \quad (45)$$

- The generalized heat equation of the Green and Nagdhi [3] model can be obtained from Eq. (14) by putting $K^* > 0, \tau_q = \tau_T = \tau_\nu = 0$. Thus we have

$$\varsigma_T \left(\frac{\partial^3 u}{\partial x \partial t^2} + \frac{\partial^3 w}{\partial z \partial t^2} \right) + l_{13} \frac{\partial^2 \varphi}{\partial t^2} + l_{14} \frac{\partial^2 \psi}{\partial t^2} + \frac{\partial^2 \theta}{\partial t^2} = l_{15} \left(\frac{\partial^2 \theta}{\partial x^2} + \frac{\partial^2 \theta}{\partial z^2} \right) + \frac{\partial^3 \theta}{\partial t \partial x^2} + \frac{\partial^3 \theta}{\partial t \partial z^2} \quad (46)$$

6. Boundary Conditions

The prescribed boundary condition is intended to be enforced at the interface $z = 0$ between the two mediums.

- (i) The pressure of the liquid and the normal stresses of the solid medium should be equal; that is

$$\frac{\partial^2 F}{\partial t^2} - 2\eta^2 \left(\frac{\partial^2 F}{\partial x^2} + \frac{\partial^2 N}{\partial x \partial z} \right) = \frac{\rho_L}{\rho} \frac{\partial^2 F_L}{\partial t^2} \quad (47)$$

- (ii) For the solid medium, the transverse component of the stress is equal to zero, that is

$$\frac{\partial^2 N}{\partial t^2} + 2\eta^2 \left(\frac{\partial^2 F}{\partial x \partial z} - \frac{\partial^2 N}{\partial x^2} \right) = 0 \quad (48)$$

- (iii) The normal displacement component of the thermoelastic solid and liquid medium is equal, that is

$$\frac{\partial F}{\partial z} - \frac{\partial N}{\partial x} = \frac{\partial F_L}{\partial z} \quad (49)$$

- (iv) The gradient of both types of void volume fraction fields is equal to zero, that is

$$\alpha \frac{\partial \varphi}{\partial z} + b_1 \frac{\partial \psi}{\partial z} = 0 \quad (50)$$

$$b_1 \frac{\partial \varphi}{\partial z} + \gamma \frac{\partial \psi}{\partial z} = 0 \quad (51)$$

- (v) The boundary condition related to thermal variation is as follows:

$$\frac{\partial \theta}{\partial z} + H^* (\theta - \theta_L) = 0 \quad (52)$$

where H^* represents the heat transmission coefficient. The index of the heat transmission confrontations within and on the surface of a body is known as the coefficient of heat transmission. The boundary is isothermal if $H^* \rightarrow \infty$ and thermally insulated if $H^* \rightarrow 0$.



7. Derivation of the Frequency Equation

Using solutions (39)-(41) in the interfacial conditions (47)-(52), a linear system of equations in E_q ($q = 1, 2, 3, 4, 5, 6$) have been attained as

$$\rho \left[(2k^2\eta^2 - \omega^2) \sum_{q=1}^4 n_q E_q + 2\iota k n_5 \eta^2 E_5 \right] = -\rho_L \omega^2 E_6 \tag{53}$$

$$-2\iota k \eta^2 \sum_{q=1}^4 n_q E_q + (2k^2\eta^2 - \omega^2) E_5 = 0 \tag{54}$$

$$\sum_{q=1}^4 n_q E_q + \iota k E_5 = -n_6 E_6 \tag{55}$$

$$\sum_{q=1}^4 n_q (A_q + l_3 B_q) E_q = 0 \tag{56}$$

$$\sum_{q=1}^4 n_q (A_q + l_8 B_q) E_q = 0 \tag{57}$$

$$\sum_{q=1}^4 (n_q - H^*) C_q E_q + H^* S_L E_6 = 0 \tag{58}$$

After doing a rigorous mathematical workout, the Eqs. (53)-(58) lead to the following frequency equation for the considered medium

$$\begin{aligned} & (2k^2\eta^2 - \omega^2)^2 (G_1 - G_2 + G_3 - G_4) + (\omega_L - \zeta) (m_1 G_1 - m_2 G_2 + m_3 G_3 - m_4 G_4) \\ & - H^* ((2k^2\eta^2 - \omega^2)^2 (G'_1 - G'_2 + G'_3 - G'_4) + (\omega_L - \zeta) (n_1 G'_1 - n_2 G'_2 + n_3 G'_3 - n_4 G'_4) - S'_L (2k^2\eta^2 - \omega^2) \\ & (G''_1 - G''_2 + G''_3 - G''_4)) = 0 \end{aligned} \tag{59}$$

where, $S'_L = \omega^2 S_L / \eta^4 n_6$, $\omega_L = \rho_L \omega^4 / \rho n_6$, $\zeta = 4k^2 \eta^4 n_5$

$$\begin{aligned} G_1 &= \begin{vmatrix} n_2 (A_2 + l_3 B_2) & n_3 (A_3 + l_3 B_3) & n_4 (A_4 + l_3 B_4) \\ n_2 (A_2 + l_8 B_2) & n_3 (A_3 + l_8 B_3) & n_4 (A_4 + l_8 B_4) \\ n_2 C_2 & n_3 C_3 & n_4 C_4 \end{vmatrix}, \\ G_2 &= \begin{vmatrix} n_1 (A_1 + l_3 B_1) & n_3 (A_3 + l_3 B_3) & n_4 (A_4 + l_3 B_4) \\ n_1 (A_1 + l_8 B_1) & n_3 (A_3 + l_8 B_3) & n_4 (A_4 + l_8 B_4) \\ n_1 C_1 & n_3 C_3 & n_4 C_4 \end{vmatrix}, \\ G_3 &= \begin{vmatrix} n_1 (A_1 + l_3 B_1) & n_2 (A_2 + l_3 B_2) & n_4 (A_4 + l_3 B_4) \\ n_1 (A_1 + l_8 B_1) & n_2 (A_2 + l_8 B_2) & n_4 (A_4 + l_8 B_4) \\ n_1 C_1 & n_2 C_2 & n_4 C_4 \end{vmatrix}, \\ G_4 &= \begin{vmatrix} n_1 (A_1 + l_3 B_1) & n_2 (A_2 + l_3 B_2) & n_3 (A_3 + l_3 B_3) \\ n_1 (A_1 + l_8 B_1) & n_2 (A_2 + l_8 B_2) & n_3 (A_3 + l_8 B_3) \\ n_1 C_1 & n_2 C_2 & n_3 C_3 \end{vmatrix}. \end{aligned}$$

Similarly, G'_q can be obtained from G_q by replacing $n_q C_q$ by C_q , $q = 1, 2, 3, 4$.

Also

$$\begin{aligned} G''_1 &= \begin{vmatrix} n_2 & n_3 & n_4 \\ n_2 (A_2 + l_3 B_2) & n_3 (A_3 + l_3 B_3) & n_4 (A_4 + l_3 B_4) \\ n_2 (A_2 + l_8 B_2) & n_3 (A_3 + l_8 B_3) & n_4 (A_4 + l_8 B_4) \end{vmatrix}, \\ G''_2 &= \begin{vmatrix} n_1 & n_3 & n_4 \\ n_1 (A_1 + l_3 B_1) & n_3 (A_3 + l_3 B_3) & n_4 (A_4 + l_3 B_4) \\ n_1 (A_1 + l_8 B_1) & n_3 (A_3 + l_8 B_3) & n_4 (A_4 + l_8 B_4) \end{vmatrix}, \\ G''_3 &= \begin{vmatrix} n_1 & n_2 & n_4 \\ n_1 (A_1 + l_3 B_1) & n_2 (A_2 + l_3 B_2) & n_4 (A_4 + l_3 B_4) \\ n_1 (A_1 + l_8 B_1) & n_2 (A_2 + l_8 B_2) & n_4 (A_4 + l_8 B_4) \end{vmatrix}, \\ G''_4 &= \begin{vmatrix} n_1 & n_2 & n_3 \\ n_1 (A_1 + l_3 B_1) & n_2 (A_2 + l_3 B_2) & n_3 (A_3 + l_3 B_3) \\ n_1 (A_1 + l_8 B_1) & n_2 (A_2 + l_8 B_2) & n_3 (A_3 + l_8 B_3) \end{vmatrix}. \end{aligned}$$

The frequency Eq. (59) exhibits complete information on the wave characteristics like the coefficient of attenuation, phase velocity, wavenumber, and many other features of waves. The limiting cases of the frequency equation are discussed as follows.

For the thermal shield case ($H^* \rightarrow 0$), the frequency Eq. (59) reduces to

$$(2k^2\eta^2 - \omega^2)^2 (G_1 - G_2 + G_3 - G_4) + (\omega_L - \zeta) (n_1 G_1 - n_2 G_2 + n_3 G_3 - n_4 G_4) = 0 \tag{60}$$



For the isothermal case ($H^* \rightarrow \infty$), the frequency Eq. (59) reduces to

$$(2k^2\eta^2 - \omega^2)^2(G'_1 - G'_2 + G'_3 - G'_4) + (\omega_L - \zeta)(n_1G'_1 - n_2G'_2 + n_3G'_3 - n_4G'_4) - (2k^2\eta^2 - \omega^2)S'_L(G''_1 - G''_2 + G''_3 - G''_4) = 0 \quad (61)$$

In the absence of liquid ($\rho_L \rightarrow 0$), the frequency Eqs. (60) and (61) reduces to

$$(2k^2\eta^2 - \omega^2)^2(G_1 - G_2 + G_3 - G_4) - \zeta(n_1G_1 - n_2G_2 + n_3G_3 - n_4G_4) = 0 \quad (62)$$

$$(2k^2\eta^2 - \omega^2)^2(G'_1 - G'_2 + G'_3 - G'_4) - \zeta(n_1G'_1 - n_2G'_2 + n_3G'_3 - n_4G'_4) = 0 \quad (63)$$

8. Method of Solution: Frequency Equation

The roots of the characteristics Eq. (36) are complex in nature, leading to the wave's phase velocity being represented as a complex value. After obtaining the roots n_j^* ; $j = 1, 2, 3, 4, 5, 6$, we get

$$c_j = \pm \frac{1}{n_j}; \quad j = 1, 2, 3, 4, 5, 6. \quad (64)$$

The six sets result in four different coupled longitudinal and one shear wave that can move through the porous solid medium with three phases and one longitudinal wave in the inviscid fluid medium. Among these five waves, the shear wave is neither attenuated nor dispersive, while the other four linked longitudinal waves are dispersive and attenuated that rely on both types of voids volume fraction fields, and temperature change.

The following relation is considered to simplify the frequency equation.

$$c_j^{-1} = v_j^{-1} + i\omega^{-1}Q_j^* \quad (65)$$

where $k = R_j^* + i\omega^{-1}Q_j^*$, Q_j^* and $R_j^* = \omega/\nu_j$ are real quantities. By using Eq. (39), the exponential of time harmonic wave solution becomes $-Q_j^*x + iR_j^*(x - \nu_j t)$, where Q_j^* and ν_j represent the coefficient of attenuation and phase velocity, respectively. Also, the characteristic roots $n_j^* = k^2(1 - \lambda_j^2 c^2)$ are evaluated with the aid of MatLab software by plugging the relation (65) in the frequency Eq. (59). Consequently, the attenuation coefficient and phase velocity have been determined respectively as $Q_j^* = \omega \text{Im}(n_j)$, $\nu_j = 1/\text{Re}(n_j)$ by plugging Eq. (65) in Eq. (64).

The vibrations of a body, in the end, come to rest, regardless of its isolation from its surroundings. This results from internal friction brought on by energy loss inside the substance. Internal friction can be calculated in both direct and indirect ways; the most popular one is to determine the ratio $\Delta W/W$. The elastic energy held in a specimen at maximum strain is denoted by W , whereas the quantity of energy wasted in it throughout a stress cycle is denoted by ΔW . This ratio is known as specific loss and is presented as

$$SL = \left| \frac{\Delta W}{W} \right| = 4\pi \left| \frac{\text{Im}(k)}{\text{Re}(k)} \right| = 4\pi \left| \frac{Q_j^*}{R_j^*} \right| = 4\pi \left| \frac{\nu_j Q_j^*}{\omega} \right| \quad (66)$$

The penetrating depth is given as

$$PD = \frac{1}{|\text{Im}(k)|} = \frac{1}{|Q_j^*|} \quad (67)$$

9. Determination of Amplitudes

By using the Eqs. (16)-(17) and (39)-(41) at the interface $z = 0$, the displacements amplitude, void volume fraction fields for both types of voids, and the temperature change have been found as

$$\begin{aligned} \tilde{U}_s &= U_s \Omega \exp \{ \iota R_j^* (x - \nu_j^* t) \}, & \tilde{W}_s &= W_s \Omega \exp \{ \iota R_j^* (x - \nu_j^* t) \}, \\ \tilde{\varphi}_s &= \Phi \Omega \exp \{ \iota R_j^* (x - \nu_j^* t) \}, & \tilde{\psi}_s &= \Psi \Omega \exp \{ \iota R_j^* (x - \nu_j^* t) \}, \\ \tilde{T}_s &= \Theta \Omega \exp \{ \iota R_j^* (x - \nu_j^* t) \}, & \tilde{U}_L &= U_L \Omega \exp \{ \iota R_j^* (x - \nu_j^* t) \}, \\ \tilde{W}_L &= W_L \Omega \exp \{ \iota R_j^* (x - \nu_j^* t) \}, & \tilde{\theta}_L &= \Theta_L \Omega \exp \{ \iota R_j^* (x - \nu_j^* t) \}; \quad j = 1, 2, 3, 4, 5, 6. \end{aligned} \quad (68)$$

Here

$$u = \tilde{U}_s, \quad w = \tilde{W}_s, \quad \varphi = \tilde{\varphi}_s, \quad \psi = \tilde{\psi}_s, \quad \theta = \tilde{\theta}_s, \quad u_L = \tilde{U}_L, \quad w_L = \tilde{W}_L, \quad \theta_L = \tilde{\theta}_L \quad \text{at the interface } z = 0.$$

Also

$$\begin{aligned} \Omega &= E_1 \exp \{ -Q_j^* x \}, \\ U_S &= ik \left(1 + \frac{E_2}{E_1} + \frac{E_3}{E_1} + \frac{E_4}{E_1} \right) - n_5 \frac{E_5}{E_1}, & W_S &= - \left(n_1 + n_2 \frac{E_2}{E_1} + n_3 \frac{E_3}{E_1} + n_4 \frac{E_4}{E_1} - ik \frac{E_5}{E_1} \right), \\ \Phi &= A_1 + A_2 \frac{E_2}{E_1} + A_3 \frac{E_3}{E_1} + A_4 \frac{E_4}{E_1}, & \Psi &= B_1 + B_2 \frac{E_2}{E_1} + B_3 \frac{E_3}{E_1} + B_4 \frac{E_4}{E_1}, \\ \Theta &= C_1 + C_2 \frac{E_2}{E_1} + C_3 \frac{E_3}{E_1} + C_4 \frac{E_4}{E_1}, & U_L &= ik \frac{E_6}{E_1}, \quad W_L = n_6 \frac{E_6}{E_1}, \quad \Theta_L = S_L \frac{E_6}{E_1} \end{aligned}$$

Using Eqs. (68) in Eqs. (47)-(51), a set of the equation has been obtained, which can be written in matrix form as

$$\begin{bmatrix} 1 & 1 & 1 & Pn_5 & R \\ -Pn_2 & -Pn_3 & -Pn_4 & 1 & 0 \\ n_2 & n_3 & n_4 & ik & n_6 \\ n_2(A_2 + l_3 B_2) & n_3(A_3 + l_3 B_3) & n_4(A_4 + l_3 B_4) & 0 & 0 \\ n_2(A_2 + l_8 B_2) & n_3(A_3 + l_8 B_3) & n_4(A_4 + l_8 B_4) & 0 & 0 \end{bmatrix} \begin{bmatrix} E_2/E_1 \\ E_4/E_1 \\ E_5/E_1 \\ E_6/E_1 \end{bmatrix} = \begin{bmatrix} -1 \\ Pn_1 \\ -n_1 \\ -n_1(A_1 + l_3 B_1) \\ -n_1(A_1 + l_8 B_1) \end{bmatrix},$$



where, $R = \frac{\rho_L \omega^2}{\rho \eta^2 S}$, $Q = \frac{2tk}{S}$, $S = (2k^2 \eta^2 - \omega^2) / \eta^2$.

The terms E_i/E_1 , $i = 2 - 6$ are given in Appendix C.

10. Numerical Results and Discussion

Numerical results obtained using MatLab software are presented here to demonstrate the analytical findings in earlier sections. Magnesium crystal-like material has been taken for scientific calculations, and the numerical values following [10], [16] are given in Table 1.

Table 1. Physical data of the material

Symbol	Value	Symbol	Value
λ	$1.5 \times 10^{10} \text{ Nm}^{-2}$	μ	$7.5 \times 10^9 \text{ Nm}^{-2}$
ρ	$2 \times 10^3 \text{ Kgm}^{-3}$	α	$8 \times 10^9 \text{ N}$
α_1	$1.2 \times 10^{10} \text{ Nm}^{-2}$	α_2	$2.21 \times 10^{10} \text{ Nm}^{-2}$
α_3	$1.23 \times 10^6 \text{ Nm}^{-2}$	α_t	$1.78 \times 10^{-5} \text{ K}^{-1}$
γ	$8.2 \times 10^9 \text{ N}$	γ_1	$2 \times 10^6 \text{ Nm}^{-2} \text{ K}^{-1}$
γ_2	$3.11 \times 10^6 \text{ Nm}^{-2}$	T_0	293 K
b	$2 \times 10^8 \text{ Nm}^{-2}$	b_1	$8.1 \times 10^6 \text{ N}$
d	$2.1 \times 10^8 \text{ Nm}^{-2}$	C_e	$1.809 \times 10^6 \text{ m}^2 \text{ s}^2 \text{ K}^{-1}$
K	$1.7 \times 10^2 \text{ Wm}^{-1} \text{ K}^{-1}$	χ_1	320 kgm^{-1}
χ_2	330 kgm^{-1}	ρ_L	$1 \times 10^3 \text{ Kgm}^{-3}$
λ_L	$2.140 \times 10^3 \text{ Nm}^{-2}$	K^*	$60 \text{ Wm}^{-1} \text{ K}^1 \text{ s}^{-1}$
C_e^*	$1.008 \text{ m}^2 \text{ s}^2 \text{ K}^{-1}$	T_0^*	293 K
$\bar{\beta}$	280	α_t^*	0.0563 K^{-1}

For time delay, the different parameters are considered as $\tau_\nu = 0.01 \text{ s}$, $\tau_T = 0.05 \text{ s}$, and $\tau_q = 0.08 \text{ s}$. Using the above value of parameters; the various graphs are plotted with respect to wavenumber corresponding to Lord-Shulman (LS) model, dual-phase-lag (DPL) model, and three-phase-lag (TPL) model. In the graphs, The LS model is represented by the solid line, the DPL model corresponds to the dotted line, and the TPL model corresponds to the dashed line.

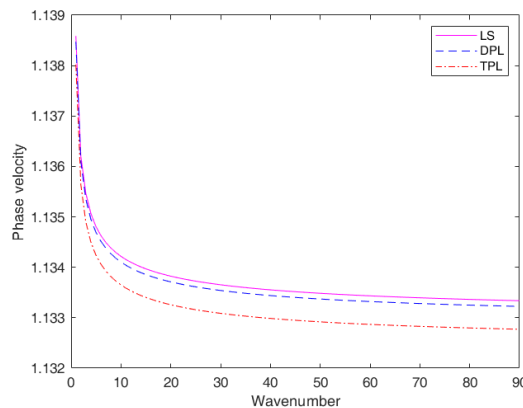


Fig. 2. Variation of phase velocity with wavenumber

Figure 2 illustrates the behaviour of phase velocity with wavenumber. The observation reveals that the phase velocity exhibits an exponential decrease with increasing wavenumber. For the small value of the wavenumber, all the curves coincide, but there is a noticeable variation in all considered models as the wavenumber increases. The LS model demonstrates phase velocities with larger magnitudes than those of the DPL and TPL models. These trends confirm that the impact of phase-lag constraints has a retreating effect on the variation of phase velocity.

The behaviour of specific loss with the wavenumber for LS, DPL, and TPL models is depicted in Figure 3. As the wavenumber increases; there is a noticeable decrease in the magnitude of specific loss. Initially, for small values of wavenumber, there is an extensive decrease in the magnitude of the specific loss, but thereafter it slightly decreases for the large wavenumber. The specific loss values for the TPL model are higher as compared to DPL and LS models. This trend shows that the phase-lag constraints perform as increasing agents.

Figure 4 illustrates the relationship between the attenuation coefficient of the waves and wavenumber. Across all the analyzed models, the attenuation coefficient's amplitude is at its minimum when the wavenumber is smaller, progressively increasing as the wavenumber increases. Notably, the TPL model exhibits a higher attenuation coefficient value compared to both the DPL and LS models. This observation suggests that the phase lag significantly influences the amplitude of the attenuation coefficient. Consequently, the phase-lag parameters act as augmenting agents for the attenuation coefficient.

Figure 5 illustrates the influence of wavenumber on the penetrating depth. The penetrating depth's amplitude diminishes as the wavenumber increases in all three considered models. In the starting range of the wavenumber, the magnitude of penetrating depth decreases sharply, but as the wavenumber progresses, the magnitude decreases at a slow rate. The penetrating depth has a greater value for the LS model than the DPL and TPL models. It can be concluded that phase-lag parameters act as a factor that decreases the magnitude of the penetrating depth.

Figures 6 and 7 depict the behaviour of horizontal and vertical surface displacements within the solid half-space with wavenumber, employing the LS, DPL, and TPL models. Notably, the magnitude of both displacement components demonstrates consistent



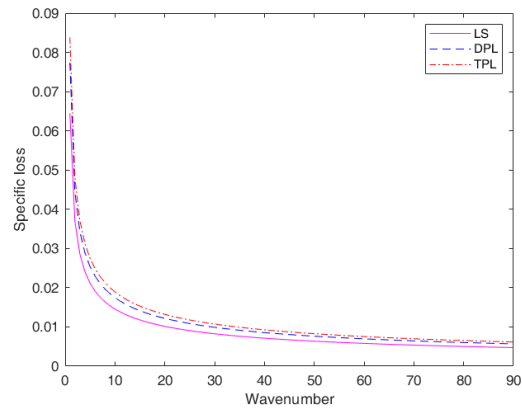


Fig. 3. Variation of specific loss with wavenumber

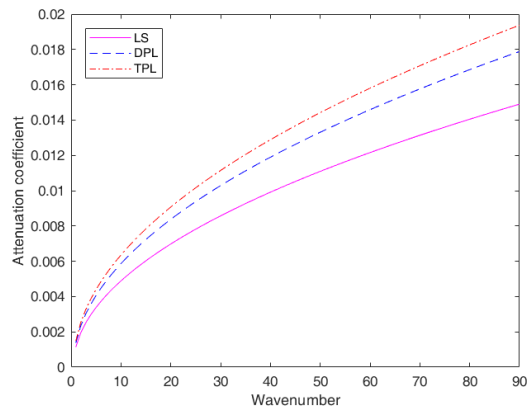


Fig. 4. Variation of attenuation coefficient with wave number

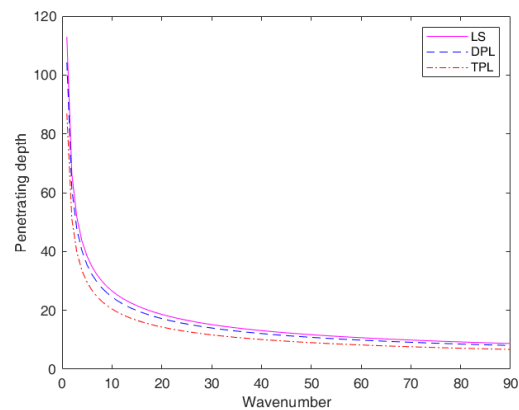


Fig. 5. Variation of penetrating depth with wave number

growth as the wavenumber increases across all considered models. Additionally, the phase lag significantly impacts the magnitude of these surface displacement components. In particular, a noteworthy observation is that both the horizontal displacement and vertical displacement components exhibit greater magnitudes in the LS model when compared to the DPL and TPL models.

Figures 8 and 9 illustrate the response of horizontal liquid displacement and vertical liquid displacement components with respect to the wavenumber. Notably, the magnitude trends of these liquid displacement components exhibit similarities to the surface displacement components within the solid half-space. However, due to inherent distinctions in their material properties and characteristics, the actual magnitude values of the liquid displacement components may differ from those observed in the solid surface displacement.

Figures 10 and 11 illustrate the behaviour of surface temperature change in solid and liquid half-space, respectively, with wavenumber. The impact of phase lags on the surface temperature change in solid and liquid half-space has also been noticed. It has been noted that with the increase in wavenumber, surface temperature change increases in both half-spaces exponentially. The amplitudes of surface temperature change are very high in a solid medium as compared to a liquid medium. Although in both the mediums, the temperature change follows the same trend, i.e., the TPL model has the highest amplitude, whereas the LS model has the lowest magnitude.



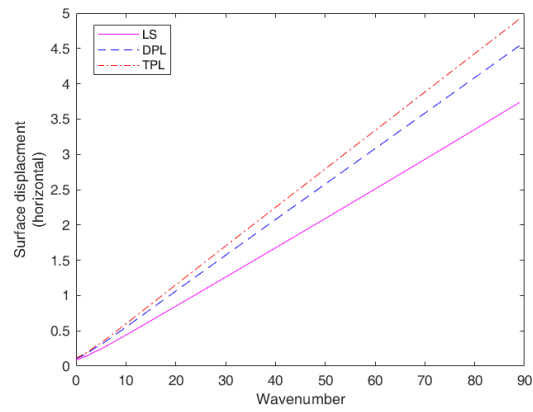


Fig. 6. Variation of horizontal surface displacement with wavenumber

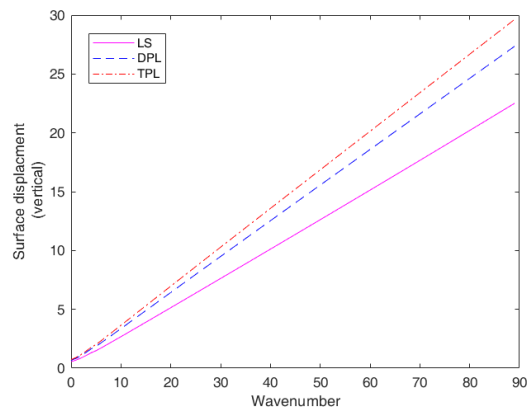


Fig. 7. Variation of vertical surface displacement with wavenumber

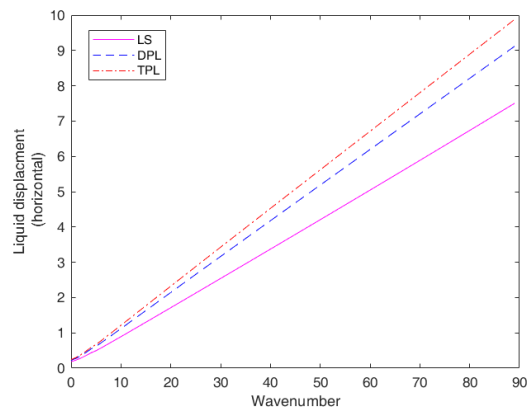


Fig. 8. Variation of horizontal liquid displacement with wavenumber

Figures 12 and 13 exhibit the plots of void volume fraction fields for both type-I, II, respectively, with varying wavenumbers in the context of the LS, DPL, and TPL models. An evident observation is that both types of void volume fraction fields experience a decline as the wavenumber increases. Initially, this decrease occurs rapidly within the lower wavenumber range, but as the wavenumber increases further, both types of void volume fraction fields exhibit a considerably slower rate of decrease. Moreover, it is worth noting that the amplitude of the void volume fraction fields is notably higher in the TPL model compared to both the DPL and LS models.

11. Conclusions

The current research delves into the investigation of plane wave propagation in an isotropic, homogeneous double porous thermoelastic solid half-space in contact with an inviscid liquid subjected to varying temperatures while accounting for three-phase lag effects. The study presents the derivation of the frequency equation and amplitude ratios in a simplified form. Furthermore, the figures showcase the influence of phase lags on the diverse physical properties of the waves. From the numerical and analytical discussion, some observations are concluded as

- In the double porous solid medium with TPL thermoelastic properties, there may exist coupling between the longitudinal



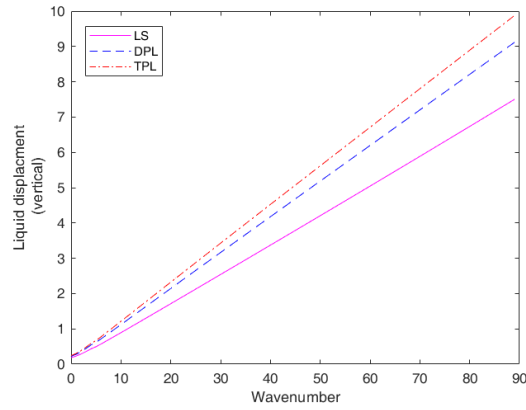


Fig. 9. Variation of vertical liquid displacement with wavenumber

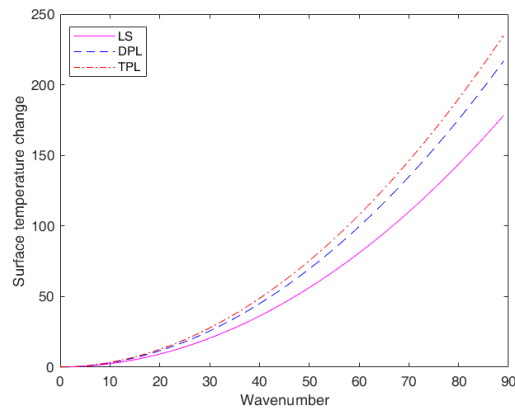


Fig. 10. Variation of surface temperature change with wavenumber

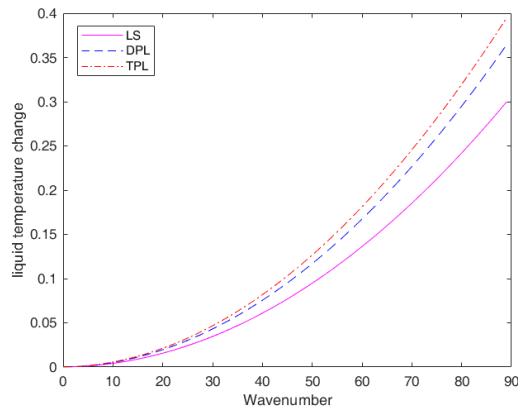


Fig. 11. Variation of liquid temperature change with wavenumber

waves, both types of void volume fraction fields, thermal waves, and shear waves. The inviscid liquid half-space may also contain one mechanical wave.

- For all the considered models, the amplitude of the penetrating depth, specific loss, and phase velocity decreases as there is an increase in wavenumber while the amplitude of the attenuation coefficient increases.
- The attenuation coefficient and specific loss have a greater value for the TPL model, and for phase velocity and penetrating depth, the LS model exhibits higher amplitude values when contrasted with the TPL model.
- The displacement components, both horizontal and vertical, temperature change, increases as the wavenumber increases. The TPL model demonstrates higher magnitudes for all these physical properties, while the LS model exhibits the minimum values.
- It can be concluded that phase-lag parameters behave as a mounting agent for both types of void volume fraction fields.



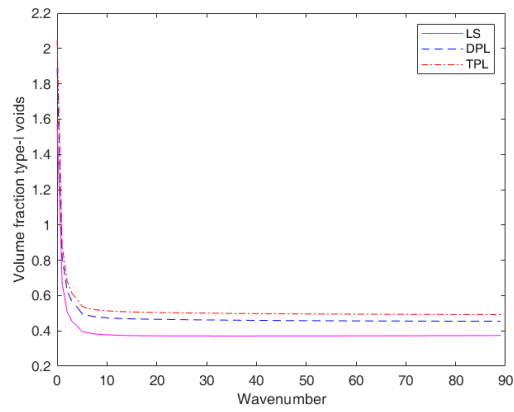


Fig. 12. Variation of volume fraction type-I voids with wavenumber

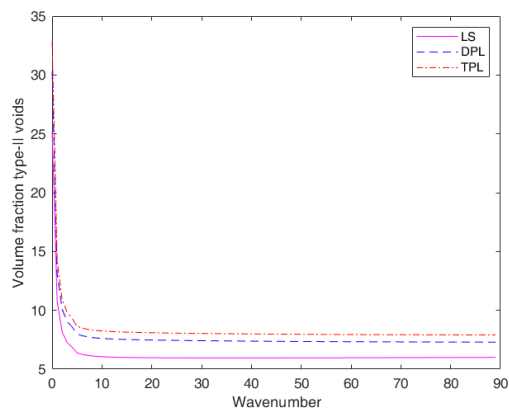


Fig. 13. Variation of volume fraction type-II voids with wavenumber

The findings from this study offer substantial potential for practical implementation in a range of disciplines. Engineers can leverage these insights to craft materials customized for specific thermal and mechanical characteristics, thereby elevating the efficacy of structural components. In the realm of hydrology, this research plays a pivotal role in elucidating the intricate dynamics of fluid-solid interactions within porous media, holding particular relevance for groundwater and reservoir engineering. Furthermore, diverse industries including ultrasonics, navigation, and electronics stand to gain advantages from enhanced models for wave propagation and heat conduction, paving the way for more efficient and advanced technologies. In summation, the wide-ranging implications of this study provide invaluable resources for improving materials and processes in numerous practical applications.

Author Contributions

All the authors contributed to the study's conception and design. Material preparation, data collection, and analysis were performed by Rajesh Kumar, Vipin Gupta and M.S. Barak. The mathematical model is developed by Vijayata Pathania and Hijaz Ahmad. The manuscript was written through the contribution of all authors. Also, all the authors read and approved the final manuscript.

Acknowledgments

Mr. Vipin Gupta is highly thankful to CSIR for the financial aid.

Conflict of Interest

The authors assert that there are no pertinent financial or non-financial conflicts of interest to disclose.

Funding

Not available.

Data Availability Statements

This manuscript has no associated data.

Nomenclature

- (a) For the thermoelastic solid half-space,
- (b) For the liquid half-space



λ, μ	Lame's constants	φ, ψ	Volume fraction field due to type-I, II voids
b, d	Voids parameters	α_t	Linear thermal expansion
ρ	Density	χ_1, χ_2	Equilibrated inertia's coefficients
C_e	Specific heat	θ	Thermal temperature
θ_0	Ambient temperature	γ_1, γ_2	Thermal constitutive coefficients
K	Thermal conductivity	K^*	Material constant
u_i	Displacement components	τ_T	Phase-lag of temperature gradient
τ_q	Phase-lag of heat flux	τ_ν	Phase-lag of thermal displacement
$\alpha, \alpha_1, \alpha_2, \alpha_3, b_1, \gamma$	Material constants		
λ_L	Lame's constant	$(u_L)_i$	Displacement components
C_e^*	Specific heat	ρ_L	Density
c_L^2	Velocity of sound	θ_L	Thermal temperature
θ_0^*	Ambient temperature	α_t^*	Coefficient of linear thermal expansion

References

- [1] Lord, H.W., Shulman, Y., A generalized dynamical theory of thermoelasticity, *J. Mech. Phys. Solids*, 1967, 15, 299–309.
- [2] Green, A.E., Lindsay, K.A., Thermoelasticity, *J. Elast.*, 1972, 2, 1–7.
- [3] Green, A.E., Naghdi, P.M., Thermoelasticity without energy dissipation, *J. Elast.*, 1993, 31, 189–208.
- [4] Tzou, D.Y., A unified field approach for heat conduction from macro- to micro-scales, *J. Heat Transfer*, 1995, 117, 8–16.
- [5] Choudhuri, S.R., On a thermoelastic three-phase-lag model, *J. Therm. Stress.*, 2007, 30, 231–238.
- [6] Nunziato, J.W., Cowin, S.C., A nonlinear theory of elastic materials with voids, *Arch. Ration. Mech. Anal.*, 1979, 72, 175–201.
- [7] Aifantis, E.C., Introducing a multi-porous medium, *Dev. Mech.*, 1977, 8, 209–211.
- [8] Iesan, D., A theory of thermoelastic materials with voids, *Acta Mech.*, 1986, 60, 67–89.
- [9] Svanadze, M., Fundamental solution in the theory of consolidation with double porosity, *J. Mech. Behav. Mater.*, 2005, 16, 123–130.
- [10] Sharma, J.N., Kumar, S., Sharma, Y.D., Propagation of rayleigh surface waves in microstretch thermoelastic continua under inviscid fluid loadings, *J. Therm. Stress.*, 2008, 31, 18–39.
- [11] Iesan, D., Quintanilla, R., On a theory of thermoelastic materials with a double porosity structure, *J. Therm. Stress.*, 2014, 37, 1017–1036.
- [12] Straughan, B., Stability and uniqueness in double porosity elasticity, *Int. J. Eng. Sci.*, 2013, 65, 1–8.
- [13] Kumar, M., Barak, M.S., Kumari, M., Reflection and refraction of plane waves at the boundary of an elastic solid and double-porosity dual-permeability materials, *Pet. Sci.*, 2019, 16, 298–317.
- [14] Kumar, R., Vohra, R., Steady state response due to moving load in thermoelastic material with double porosity, *Mater. Phys. Mech.*, 2020, 44, 172–185.
- [15] Sharma, J.N., Pathania, V., Generalized thermoelastic lamb waves in a plate bordered with layers of inviscid liquid, *J. Sound Vib.*, 2003, 268, 897–916.
- [16] Singh, D., Kumar, D., Tomar, S.K., Plane harmonic waves in a thermoelastic solid with double porosity, *Math. Mech. Solids*, 2020, 25, 869–886.
- [17] Chirita, S., Arusoae, A., Thermoelastic waves in double porosity materials, *Eur. J. Mech. - A/Solids*, 2021, 86, 104177.
- [18] Pathania, V., Dhiman, P., On lamb type waves in a porothermoelastic plate immersed in the inviscid fluid, *Waves in Random and Complex Media*, 2021, 2021, 1–27.
- [19] Svanadze, M., Potential method in the coupled theory of elastic double-porosity materials, *Acta Mech.*, 2021, 232, 2307–2329.
- [20] Pathania, V., Joshi, P., Waves in thermoelastic solid half-space containing voids with liquid loadings, *ZAMM - J. Appl. Math. Mech. / Zeitschrift für Angew. Math. und Mech.*, 2021, 101, 1–19.
- [21] Barak, M.S., Kumar, R., Kumar, R., Gupta, V., Energy analysis at the boundary interface of elastic and piezothermoelastic half-spaces, *Indian J. Phys.*, 2023, 2023.
- [22] Barak, M.S., Kumar, R., Kumar, R., Gupta, V., The effect of memory and stiffness on energy ratios at the interface of distinct media, *Multidiscip. Model. Mater. Struct.*, 2023, 19, 464–492.
- [23] Gupta, V., Barak, M.S., Quasi-p wave through orthotropic piezo-thermoelastic materials subject to higher order fractional and memory-dependent derivatives, *Mech. Adv. Mater. Struct.*, 2023, 0, 1–15.
- [24] Gupta, V., Kumar, R., Kumar, R., Barak, M.S., Energy analysis at the interface of piezo/thermoelastic half spaces, *Int. J. Numer. Methods Heat Fluid Flow*, 2023, 33, 2250–2277.
- [25] Biswas, S., Fundamental solution of steady oscillations for porous materials with dual-phase-lag model in micropolar thermoelasticity, *Mech. Based Des. Struct. Mach.*, 2019, 47, 430–452.
- [26] Hobiny, A., Abbas, I., Generalized thermoelastic interaction in a two-dimensional porous medium under dual phase lag model, *Int. J. Numer. Methods Heat Fluid Flow*, 2020, 30, 4865–4881.
- [27] Quintanilla, R., Racke, R., A note on stability in three-phase-lag heat conduction, *Int. J. Heat Mass Transf.*, 2008, 51, 24–29.
- [28] Shaw, S., Mukhopadhyay, B., Analysis of rayleigh surface wave propagation in isotropic micropolar solid under three-phase-lag model of thermoelasticity, *Eur. J. Comput. Mech.*, 2015, 24, 64–78.
- [29] Kalkal, K.K., Kadian, A., Kumar, S., Three-phase-lag functionally graded thermoelastic model having double porosity and gravitational effect, *J. Ocean Eng. Sci.*, 2021, 2021.
- [30] Biswas, S., Three-dimensional vibration analysis of porous cylindrical panel with a three-phase-lag model, *Waves in Random and Complex Media*, 2021, 31, 1879–1904.
- [31] Biot, M.A., Thermoelasticity and irreversible thermodynamics, *J. Appl. Phys.*, 1956, 27, 240–253.

ORCID iD

Rajesh Kumar  <https://orcid.org/0000-0003-2065-1372>

Vijayata Pathania  <https://orcid.org/0000-0003-3842-0759>

Vipin Gupta  <https://orcid.org/0000-0002-5238-1963>

M.S. Barak  <https://orcid.org/0000-0001-9947-000X>

Hijaz Ahmad  <https://orcid.org/0000-0002-5438-5407>



© 2023 Shahid Chamran University of Ahvaz, Ahvaz, Iran. This article is an open access article distributed under the terms and conditions of the Creative Commons Attribution-NonCommercial 4.0 International (CC BY-NC 4.0 license) (<http://creativecommons.org/licenses/by-nc/4.0/>)



How to cite this article: Rajesh Kumar, Vijayata Pathania, Vipin Gupta, M.S. Barak, Hijaz Ahmad. Thermoelastic Modeling with Dual Porosity Interacting with an Inviscid Liquid, J. Appl. Comput. Mech., 10(1), 2024, 111-124. <https://doi.org/10.22055/jacm.2023.44488.4221>

Publisher’s Note Shahid Chamran University of Ahvaz remains neutral with regard to jurisdictional claims in published maps and institutional affiliations.

Appendix A

$$\begin{aligned}
 J_0 &= (l_8 - l_3)d_{55}, \\
 J_1 &= (l_8 - l_3)(d_{51} + d_{56}) + d_{55}(d_{43} - d_{33} - l_2l_4 + l_2l_9 + d_{11}(l_8 - l_3) + l_8d_{32} - l_3d_{42} - l_1l_3l_9 + l_1l_4l_8), \\
 J_2 &= d_{51}(d_{43} - d_{33} + l_2(l_{12} - l_7) + l_8(d_{32} + l_1l_7) - l_3(d_{42} + l_1l_{12})) + d_{52}(l_8 - l_3) + d_{53}(l_8(l_4 - l_7) + l_3(l_{12} - l_9)) + d_{54}(l_7 - l_4 + l_9 - l_{12}) \\
 &\quad + d_{55}(l_2(d_{31} - d_{41}) + d_{11}(d_{43} - d_{33} + l_8d_{32} - l_3d_{42}) + d_{32}(d_{43} + l_2l_9) - d_{42}(d_{33} + l_2l_4) + l_1(l_3d_{41} + l_4d_{43} - l_8d_{31} - l_9d_{33})) \\
 &\quad + d_{56}(d_{43} - d_{33} + l_2(l_9 - l_4) + d_{11}(l_8 - l_3) + l_8(d_{32} + l_1l_4) - l_3(d_{42} + l_1l_9)), \\
 J_3 &= d_{51}(d_{32}(d_{43} + l_2l_{12}) - d_{42}(d_{33} + l_2l_7) + l_1(l_7d_{43} - l_{12}d_{33})) + d_{52}(d_{43} - d_{33} + l_2(l_{12} - l_7) + l_8(d_{32} + l_1l_7) - l_3(d_{42} + l_1l_{12})) \\
 &\quad + d_{53}(d_{33}(l_{12} - l_9) + d_{43}(l_4 - l_7) + d_{11}(l_3l_{12} - l_7l_8) + l_2(l_4l_{12} - l_7l_9) - l_8d_{31} + l_3d_{41}) + d_{54}(d_{31} - d_{41} + d_{11}(l_7 - l_{12})) \\
 &\quad + d_{32}(l_9 - l_{12}) + d_{42}(l_7 - l_4) + l_1(l_7l_9 - l_1l_{12})) + d_{55}(d_{33}(l_1d_{41} - d_{11}d_{42}) + d_{31}(l_2d_{42} - l_1d_{43}) + d_{32}(d_{11}d_{43} - l_2d_{41})) \\
 &\quad + d_{56}(d_{31}(l_2 - l_1l_8) + d_{41}(l_1l_3 - l_2) + d_{11}(d_{43} - d_{33} - l_3d_{42}) + d_{32}(d_{43} + l_2l_9 + l_8d_{11}) - d_{42}(d_{33} + l_2l_4) + l_1(l_4d_{43} - l_9d_{33})), \\
 J_4 &= d_{52}(d_{32}(d_{43} + l_2l_{12}) - d_{42}(d_{33} + l_2l_7) + l_1(l_7d_{43} - l_{12}d_{33})) + d_{53}(d_{41}(d_{33} + l_2l_7) - d_{31}(d_{43} + l_2l_{12}) + d_{11}(l_{12}d_{33} - l_7d_{43})) \\
 &\quad + d_{54}(d_{31}(d_{42} - l_1l_{12}) - d_{41}(d_{32} + l_1l_7) + d_{11}(l_7d_{42} - l_{12}d_{32})) + d_{56}(d_{33}(l_1d_{41} - d_{11}d_{42}) + d_{31}(l_2d_{42} - l_1d_{43}) + d_{32}(d_{11}d_{43} - l_2d_{41})).
 \end{aligned}$$

Appendix B

$$\begin{aligned}
 A_q &= ((l_8(l_4 - l_7) + l_3(l_{12} - l_9))n_q^4 + (d_{33}(l_{12} - l_9) + d_{43}(l_4 - l_7) + d_{11}(l_3l_{12} - l_7l_8) + l_2(l_4l_{12} - l_7l_9) + l_3d_{41} - l_8d_{31})n_q^2 \\
 &\quad + d_{41}(d_{33} + l_2l_7) - d_{31}(d_{43} + l_2l_{12}) + d_{11}(l_{12}d_{33} - l_7d_{43}))/L^*, \\
 B_q &= ((l_7 - l_4 + l_9 - l_{12})n_q^4 + (d_{31} - d_{41} + d_{11}(l_7 - l_{12}) + d_{32}(l_9 - l_{12}) + d_{42}(l_7 - l_4) + l_1(l_7l_9 - l_4l_{12}))n_q^2 + d_{31}(d_{42} + l_1l_{12}) \\
 &\quad - d_{41}(d_{32} + l_1l_7) + d_{11}(l_7d_{42} - l_{12}d_{32}))/L^*, \\
 C_q &= ((l_8 - l_3)n_q^6 + (d_{43} - d_{33} + l_2(l_9 - l_4) + d_{11}(l_8 - l_3) + l_8(d_{32} + l_1l_4) - l_3(d_{42} + l_3l_9))n_q^4 + (l_2(d_{31} - d_{41}) + d_{11}(d_{43} - d_{33}) \\
 &\quad + d_{32}(d_{43} + l_2l_9 + l_8d_{11}) - d_{42}(d_{31} + l_2l_4 + l_3d_{11}) + l_1(l_3d_{41} - l_9d_{33} + l_4d_{43} - l_8d_{31}))n_q^2 + d_{31}(l_2d_{42} - l_1d_{43}) \\
 &\quad + d_{41}(l_1d_{33} - l_2d_{32}) + d_{11}(d_{32}d_{43} - d_{33}d_{42}))/L^*, \\
 L^* &= (l_8 - l_3)n_q^4 + (d_{43} - d_{33} - l_2(l_7 - l_{12}) + l_8(d_{32} + l_1l_7) - l_3(d_{42} + l_1l_{12}))n_q^2 + d_{32}(d_{43} + l_2l_{12}) - d_{33}(d_{42} + l_1l_{12}) + l_7(l_1d_{43} - l_2d_{42}).
 \end{aligned}$$

Appendix C

$$\begin{aligned}
 E_2/E_1 &= ((A_3B_1 - A_1B_3)n_1n_3n_6 + (A_1B_4 - A_4B_1)n_1n_4n_6 + (A_4B_3 - A_3B_4)n_3n_4n_6 + (A_1B_3 - A_3B_1 + A_4B_1 + A_4B_1 \\
 &\quad - A_1B_4 + A_3B_4 - A_4B_3 + P_{ik}(A_1B_3 - A_3B_1 + A_4B_1 - A_1B_4 + A_3B_4 - A_4B_3))Rn_1n_3n_4 \\
 &\quad + (A_3B_1 - A_1B_3 + A_1B_4 - A_4B_1 + A_4B_3 - A_3B_4)P^2n_1n_2n_4n_5n_6)/L^{**}, \\
 E_3/E_1 &= ((A_1B_2 - A_2B_1)n_1n_2n_6 + (A_4B_1 - A_1B_4)n_1n_4n_6 + (A_2B_4 - A_4B_2)n_2n_4n_6 + (A_2B_1 - A_1B_2 + A_1B_4 - A_4B_1 \\
 &\quad + A_4B_2 - A_2B_4 + P_{ik}(A_2B_1 - A_1B_2 + A_1B_4 - A_4B_1 + A_4B_2 - A_2B_4))Rn_1n_2n_4 + (A_1B_2 - A_2B_1 + A_4B_1 - A_1B_4 \\
 &\quad + A_2B_4 - A_4B_2)P^2n_1n_2n_4n_5n_6)/L^{**}, \\
 E_4/E_1 &= ((A_2B_1 - A_1B_2)n_1n_2n_6 + (A_1B_3 - A_3B_1)n_1n_3n_6 + (A_3B_2 - A_2B_3)n_2n_3n_6 + (A_1B_2 - A_2B_1 + A_3B_1 - A_1B_3 \\
 &\quad + A_2B_3 - A_3B_2 + P_{ik}(A_1B_2 - A_2B_1 + A_3B_1 - A_1B_3 + A_2B_3 - A_3B_2))Rn_1n_2n_3 + (A_2B_1 - A_1B_2 + A_1B_3 \\
 &\quad - A_3B_1 + A_3B_2 - A_2B_3)P^2n_1n_2n_3n_5n_6)/L^{**}, \\
 E_5/E_1 &= Pn_6((A_1B_2 - A_2B_1 + A_3B_1 - A_1B_3 + A_2B_3 - A_3B_2)n_1n_2n_3 + (A_2B_1 - A_1B_2 + A_1B_4 - A_4B_1 + A_4B_2 - A_2B_4)n_1n_2n_4 \\
 &\quad + (A_1B_3 - A_3B_1 + A_4B_1 - A_1B_4 + A_3B_4 - A_4B_3)n_1n_3n_4 + (A_3B_2 - A_2B_3 + A_2B_4 - A_4B_2 + A_3B_4 + A_4B_3))/L^{**}, \\
 E_6/E_1 &= (P_{ik} + 1)((A_2B_1 - A_1B_2 + A_1B_3 - A_3B_1 + A_3B_2 - A_2B_3)n_1n_2n_3 + (A_1B_2 - A_2B_1 + A_4B_1 - A_1B_4 + A_2B_4 - A_4B_2)n_1n_2n_4 \\
 &\quad + (A_3B_1 - A_1B_3 + A_1B_4 - A_4B_1 + A_4B_3 - A_3B_4)n_1n_3n_4 + (A_2B_3 - A_3B_2 + A_4B_2 - A_2B_4 - A_3B_4 - A_4B_3))/L^{**}, \\
 L^{**} &= (A_2B_3 - A_3B_2)n_2n_3n_6 + (A_4B_2 - A_2B_4)n_2n_4n_6 + (A_3B_4 - A_4B_3)n_3n_4n_6 + (A_3B_2 - A_2B_3 + A_2B_4 - A_4B_2 + A_3B_4 \\
 &\quad - A_4B_3 + P_{ik}(A_3B_2 - A_2B_3 + A_2B_4 - A_4B_2 + A_4B_3 - A_3B_4))Rn_2n_3n_4 + (A_2B_3 - A_3B_2 + A_4B_2 - A_2B_4 + A_3B_4 \\
 &\quad - A_4B_3)P^2n_1n_2n_3n_5n_6.
 \end{aligned}$$

